EXPERIMENTAL DEVELOPMENT OF POROSITY IN CARBONATE ROCKS UNDER SIMULATED DEEP BURIAL CONDITIONS

PART I. OOMOLDIC POROSITY IN MISSISSIPPIAN OOLITIC LIMESTONE

BY

David W. RICH and **Albert V. CAROZZI** [1]

ABSTRACT

Initial experimentation under conditions simulating deep burial have led to the development of oomoldic porosity in a low permeability oolitic calcarenite from the Mississippian of Illinois, U.S.A. A specially designed triaxial apparatus was used that permitted circulation of pore fluid (CO_2-charged water) under constant vertical pressure, lateral confining pressure and temperature. Burial under non-hydrostatic conditions of 10,000 feet (3,050 m) was simulated by a vertical (axial) pressure of 10,150 psi (70 MPa), a lateral confining pressure of 8,700 psi (60 MPa), and a pore pressure of 5,800 psi (40 MPa). All pressures were held constant throughout testing and the temperature was maintained at 75°F (24°C).

A series of systematic tests have revealed that variations in specimen configuration and orientation, and differences in CO_2 concentration have little or no effect, but that variations of pore pressure differential change the final outcome of the tests. Channeling, which destroys most of the previously developed fabric-selective dissolution textures, involves a mechanical bursting of areas of the specimen previously weakened by dissolution and is directly related to the maximum value of ΔP_p near the end of the test.

RÉSUMÉ

Sous des conditions de simulation d'un enfouissement profond, des expériences préliminaires ont conduit à la formation de porosité secondaire oomoldique dans une calcarénite oolithique du Mississippien de l'Illinois, U.S.A. On a utilisé un appareil triaxial spécialement construit pour permettre la circulation d'un fluide interstitiel (eau chargée de CO_2), sous pression verticale, pression latérale de confinement et température constantes. Un enfouissement de 10.000 pieds (3050 mètres) sous des conditions non-hydrostatiques a été simulé par une pression verticale (axiale) de 713,5 kg/cm^2

[1] Department of Geology, University of Illinois at Urbana-Champaign, Urbana, Illinois, 61801, U.S.A. This paper is part of a Ph. D. thesis completed by D. W. R. under the supervision of A.V.C. and submitted to the Graduate College in 1980.

This research was supported by grants from Petróleo Brasileiro S.A. PETROBRÁS, Shell Aids program of the Shell Companies Foundation and American Association of Petroleum Geologists which are gratefully acknowledged.

(70 MPa), une pression latérale de confinement de 611,6 kg/cm² (60 MPa), et une pression interstitielle de 407,7 kg/cm² (40 MPa). Toutes les pressions ont été maintenues constantes durant les expériences, et la température a été de 75°F (24°C).

Une série d'expériences systématiques ont montré que la forme et l'orientation de l'échantillon ainsi que les différences de concentration en CO_2 ont peu ou pas d'effet, tandis que les variations du différentiel de pression interstitielle modifient le résultat final des expériences. La formation de chenaux, qui détruisent en grande partie les effets de dissolution engendrés antérieurement et sélectifs par rapport à la texture de la roche, implique une rupture mécanique des parties de l'échantillon antérieurement affaiblies par la dissolution. La chenalisation paraît être une fonction directe de la valeur maximale de ΔP_p pendant la phase finale de l'expérience.

INTRODUCTION

In recent papers (DONATH, CAROZZI, FRUTH and RICH, 1976, 1977 and 1980) we have reported the first experimental development of oomoldic porosity in a low permeability oolitic calcarenite from the Mississippian of Illinois under conditions simulating deep burial.

This simulation was obtained by placing jacketed cylindrical specimens of oolitic calcarenite in a specially designed triaxial apparatus that permits circulation of pore fluid (CO_2-charged water) under constant pressure while subjecting the rock specimen to constant vertical pressure, lateral confining pressure, and temperature. Burial conditions of 10,000 ft (3,050 m) were simulated by an axial pressure of 10,150 psi (70 MPa), a lateral confining pressure of 8,700 psi (60 MPa), and a pore pressure of 5,800 psi (40 MPa). All pressures were held constant throughout the tests and the temperature was maintained at 75°F (24°C).

The results obtained indicate that fabric-selective secondary porosity can be developed in tight carbonate rocks by circulating fluids under conditions characteristic of deep burial, that is, after pervasive cementation and after mineralogic stability have occurred. In the tested oolitic calcarenite, secondary porosity was developed and permeability was enhanced significantly by the centripetal preferential dissolution of the microporous cortical layers of the ooids, development of pore throats at the point contacts between ooids, and, ultimately by the removal of nuclei to produce oomoldic porosity.

The initial tests seemed to show that variations in specimen configuration and orientation, differences in CO_2 concentration, and variations of pore pressure differential had no appreciable influence on the dissolution effects, only on the solution rates with respect to the last two factors. A detailed evaluation of the effects of these important parameters by means of a series of systematic tests (RICH, 1980) is presented in this paper. It confirms the preliminary data on specimen configuration and orientation, and on differences of CO_2 concentration, but has disclosed an influence of the variations of pore pressure differential on the dissolution effects.

GEOLOGIC SIGNIFICANCE OF THE INITIAL EXPERIMENTS

Inasmuch as mineralogy, CO_2 concentration, fluid circulation rate, and specimen configuration have not been controlling factors, we conclude that the experimental development of fabric-selective secondary porosity is entirely the result of fabric and textural variations within components of the tested oolitic calcarenite. Our results demonstrate, further, that such fabric-selective secondary porosity can be developed in carbonate rocks of low permeability under conditions of deep burial diagenesis. Recent research on sandstone diagenesis (SCHMIDT and MCDONALD, 1979) have shown that secondary porosity can develop at depths of the order of 10,000 feet (3,050 m) and more, mostly by a process of decarbonatization affecting cements and grains. This secondary leaching occurs at depths and temperatures which include the "window" of liquid hydrocarbon generation, and it is thought to be related to changes in the chemistry of the circulating waters, mainly enrichment in CO_2, which results from the decarboxylation of organic matter and occur during the first diagenetic phase of dewatering of basinal shales.

The abundance of CO_2 in the subsurface appears also responsible for the generation of *late* secondary porosity in carbonate rocks and for the transport of significant amounts of carbonate that cement other units elsewhere in the sedimentary sequence. In essence, we are observing the effects of a multiphase process that combines the generation of secondary porosity with episodes of cementation, all having taken place during subsidence and having subsequently been modified by structural deformation. The CO_2-bearing solutions responsible for this arise from the deepest parts of the basin and ascend toward the margins. If the pathways of such migration could be reconstructed, the location of potential reservoir rocks might be predicted.

SYSTEMATIC TESTING

A series of eleven tests were performed on the same rock type as used in the initial experiments in order to systematically evaluate the effects of the following factors: specimen orientation, duration of tests, variations of pCO_2 and variations of ΔP_p.

Apparatus Used

The apparatus (Fig. 1) consists of a triaxial deformation tester of the type used in structural geology which has been modified to permit fluid to be circulated through the specimen, which consists of a cylinder of limestone about ½ inch (1.27 cm) in diameter and height. The simplified schematic diagram of the apparatus illustrated in Figure 2 shows the parts of the machine used for solution preparation and circulation, while the hydraulic systems for specimen confining fluid and axial load have been omitted for clarity.

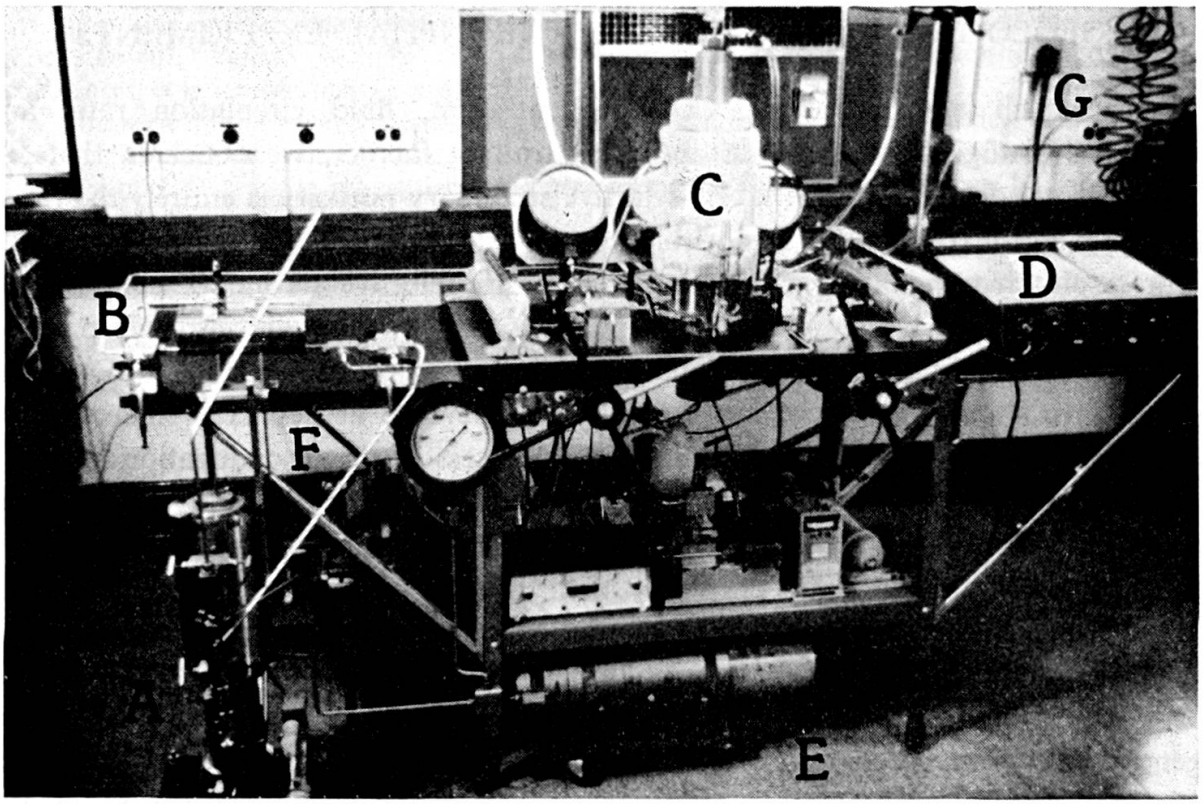

FIG. 1. — Experimental test apparatus. A: circulator; B: pore fluid sampler; C: pressure vessel; D: X-Y recorder; E: intensifier-accumulator; F: gear pump; G: source of CO_2.

The specimen confinement system is composed of a thick-walled tool steel pressure vessel rated at 30,000 psi which holds a reservoir of silicone fluid which is pressurized to provide a horizontal confining pressure of 8700 psi to simulate the rock in the subsurface adjacent to the specimen. Through the top and bottom of the vessel are inserted a piston and an anvil which have been drilled through so that they may transmit fluids to and from the specimen, and which are separated from the ends of the specimen by a metal spreader disc, a sheet of filter paper, and a porous disc made of carborundum, which together spread out the flow during testing to discourage channeling near a singel inlet (see Fig. 2, inset). The specimen is surrounded on the sides by a plastic jacket to isolate the sample pore fluid from the confining fluid. During the test the piston and anvil are forced against the ends of the specimen hydraulically to simulate an axial load slightly in excess of the confining pressure, representing burial under non-hydrostatic conditions at a depth of about 10,000 feet (3 km). The temperature during testing was maintained at 25°C rather than elevated to simulate burial conditions because the effect would be to decrease the $CaCO_3$ solubility and possibly also the amount of dissolution.

The pore fluid for circulation through the specimen was prepared and stored in a stainless steel pressure vessel called the circulator, which was also used to provide

a differential pressure for circulation. The circulator consists of an upper chamber containing the pore fluid and a lower chamber containing hydraulic fluid. Each chamber has a piston separating it into two sections, and the pistons can move up and down the length of the chambers. The two pistons are rigidly connected by a rod

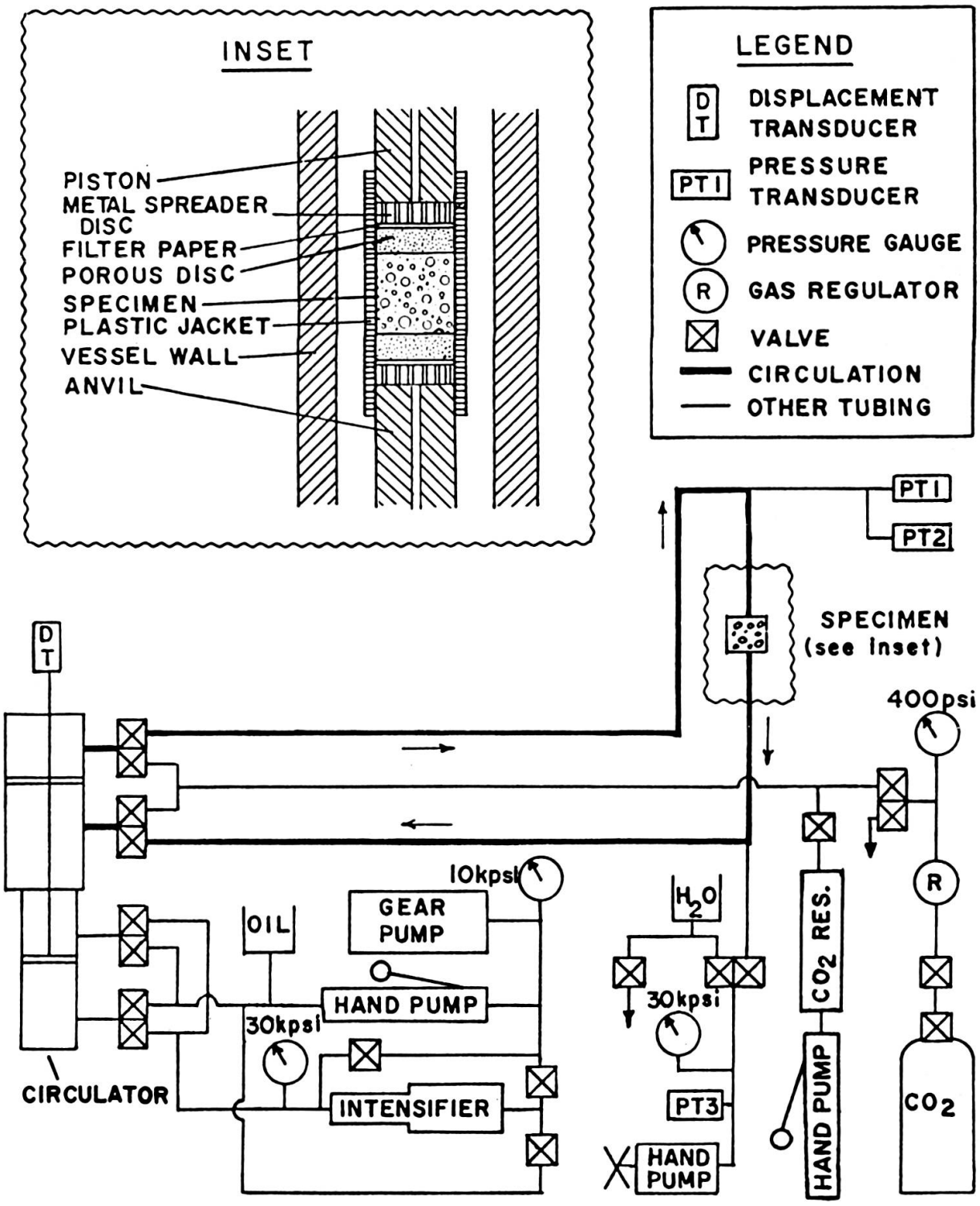

FIG. 2. — Schematic diagram of the experimental test apparatus.
The specimen confinement and load systems have been omitted for clarity.

which passes through an O-ring seal between the two chambers and another at the top of the upper chamber, allowing measurement of the piston displacement. The lower chamber is connected to a hydraulic system consisting of a multiple-rate gear pump, a hand pump, an intensifier (used to increase the pressure coming out of the pumps, allowing lower pump operating pressures), an oil reservoir and two pressure gauges, one at the output of the pumps and one at the output of the intensifier. This hydraulic system is used to move the lower piston up or down, which moves the upper piston, allowing circulation of pore fluid in either direction.

The upper chamber of the circulator is connected to the specimen for circulation and to supplies of CO_2 and H_2O for preparation of the pore fluid. The CO_2 is supplied from a gas bottle through a regulator, and the line has a pressure gauge and a bleed-off valve. The water supply is a plastic reservoir bottle which is filled with distilled, evacuated water for each test, and which is connected to a pressure gauge, a pressure transducer, a bleed-off valve and a calibrated hand pump.

The system is electronically monitored during testing with pressure and displacement transducers and chart recorders. The axial load and any length changes of the specimen are monitored by a pressure and a displacement transducer and recorded on a two-axis chart recorder. The movement of the circulator piston is also recorded with a displacement transducer and chart recorder and is used to monitor the amount of fluid circulated. The pore fluid pressure is measured with three pressure transducers, two at the inlet to the specimen (PT1 and PT2 in Fig. 2), and one connected to the outlet (PT3). One of the inflow pressure transducers and the outflow transducer are electronically bridged (subtracted) and the difference (ΔP_p) is recorded on a strip chart recorder against time, along with the signal from the second inflow transducer, so that $P_{p\,(in)}$ and ΔP_p are known and $P_{p\,(out)}$ can be calculated. The ΔP_p signal can be used to activate the gear pump to move the circulator pistons, so that the ΔP_p can be maintained automatically at some desired value, or the gear pump can be allowed to run continuously, depending upon the specimen permeability and the type of test to be run.

Material Used in Testing

The material used in the experimentation is designated as OR4A. It belongs to the Ste. Genevieve Limestone, Upper Valmeyeran, Mississippian and was collected at Western Materials Co. Quarry, Orleans, Orange County, Indiana. It is a moderately well-sorted and slightly compacted oolitic calcarenite with microporous ooids showing typical concentric structure (Plate 1, Figs. 1 and 2). The microporosity (Plate 1, Fig. 3) consists of irregular equant pores 1-3 μm in size which are located in between the rhombic to anhedral carbonate crystals of about the same size which make up the ooid cortex. In places the micropores become platy, similar to those found in dolomites (Wardlaw, 1976) or tubular. The platy

or tubular micropores, which are 0.1 μm or less in their short dimension, act as constrictions between the larger equant micropores and are called "pore throats".

Some of the bioclasts also display microporosity, for instance the foraminifer *Endothyra* sp. (Plate 1, Figs. 5 and 6) has an ultrastructure very similar in appearance to that of the ooid cortical material.

The rock displays two generations of cement, the first is an irregular bladed rim cement and the second an equant sparite, with compaction and a slight period of dissolution having occurred in the interim. Located between the cement crystals are pores 20-125 μm in size which connect the microporosity of adjacent ooids, acting as permeability bridges across the massive sparite (Plate 1, Fig. 4).

The sample has an average porosity of 13.8%, and the capillary pressure curve (Fig. 3) indicates that about 95% of the porosity is smaller than 0.5 μm and 60% is between 0.075 and 0.2 μm, or the entrance of mercury is blocked by pores of this size. Since the greatest volume of the microporosity viewed with the S.E.M. was in the range of 1-5 μm, it is concluded that the pressure of mercury invasion is controlled by the size of the pore throats rather than the size of the average pore. The permeabilities are low for the same reason. The horizontal ones average <1.9 md (gas) and 0.032 md (liquid) while the vertical are <1.9 md (gas) and 0.028 md (liquid).

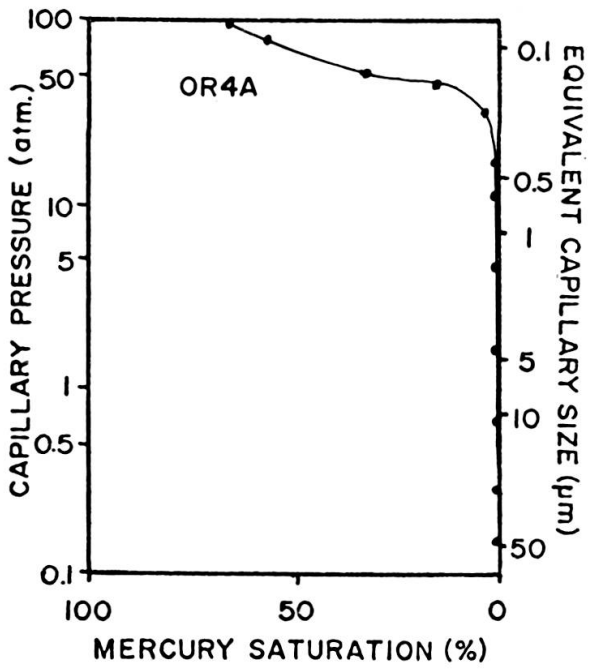

FIG. 3. — Mercury injection capillary pressure curve for sample OR4A.

X-ray diffraction analysis indicated the presence of a single major phase, low-Mg calcite, and a minor amount of quartz. The chemical composition of this rock is greater than 98% $CaCO_3$, with the rest mostly $MgCO_3$, SiO_2 and Al_2O_3 (Carr, 1973). The rock is very homogeneous, which together with its purity make it ideal for testing and other petrophysical studies (HISELER and CAROZZI, 1978).

Preparation Procedure

The sample was slabbed with a diamond saw and cored with a ½ inch (nominal) diamond core barrel. The cores were cut to about ½ inch in length and the ends ground flat and perpendicular to the sides. Prior to testing each core was weighed dry, then saturated with distilled water and weighed again. The exact length and

diameter were measured, and porosity values were calculated from the bulk density using a density for calcite of 2.71 g cc^{-1} and from the weight change upon saturation. The porosity calculated from volume and density (Φ_v) represents the total porosity, while that calculated from water saturation (Φ_s) represents the effective porosity. The saturation porosity was consistently less than the volume porosity by an average of 2.4%, indicating that this amount of porosity was non-interconnected on a scale which would allow water to enter with the pressure difference used during saturation.

Experimental Procedure

The procedure for running all tests was basically the same. After the specimen core had been prepared as described in the previous section, the porous discs, the filter paper and the plastic jacket were weighed, then the specimen assembly, including the piston and anvil, the specimen and jacket and the metal spreader discs, porous discs and filter paper, was saturated with water and placed inside the triaxial tester, and high pressure tubing was attached connecting the piston and anvil with the upper and lower sections of the upper chamber of the circulator. The circulator, which has a volume of 1080 cc, was then filled with CO_2 to the desired pressure (200 psi for tests 1, 2, 3, 4, 6, and 8, and 100 psi for tests 5, 7, 9, 10 and 11), then the CO_2 was forced into the CO_2 reservoir as the circulator was filled with distilled water which had been degassed by evacuation. The CO_2 was then forced back into the circulator and allowed to dissolve in the water. The CO_2-H_2O mixture was then agitated and moved to the top section of the upper chamber of the circulator in preparation for circulation. After seating the specimen by moving the anvil up to take up any slack in the specimen assembly, the confining pressure was pumped up to 8700 psi and the specimen reseated to provide the axial load. The pore pressure was then increased to 5800 psi by forcing more distilled water into the system with the hand pump, and a small amount of differential pore pressure was placed across the specimen by slightly advancing the circulator pistons with the hydraulic fluid hand pump. This was done to take up any slack in the gear pump and intensifier. Then the gear pump, routed through the intensifier, was turned on, increasing the pressure in the lower section of the lower chamber of the circulator, causing the pistons to move upward and pore fluid to flow from the upper section of the upper chamber of the circulator through the specimen and into the lower section of the upper chamber. The initial tests allowed the ΔP_p to increase at a rate determined by the pump gear and the permeability of the specimen. For tests 9 and 11, automatic controls were used to maintain the ΔP_p at a constant value. After testing, the specimen was removed from the apparatus, dried in an oven at 100°C for one hour, allowed to cool, and weighed, and the amount of porosity gain was calculated from the weight loss. The tested specimen was then impregnated with blue resin and thin sections were prepared for petrographic study. The pore pressure differential and amount

of fluid circulated were plotted against time for each test, and from these the relative permeability changes throughout the test were calculated and plotted also. The absolute permeability could not be calculated because no data on the viscosity of carbonic acid under test conditions could be found in the specialized literature. Therefore, an arbitrary value of one centipoise was assigned to the viscosity, then the permeabilities were calculated by using the following equation which is a rearrangement of Darcy's law:

$$k = \frac{1000\, Q\, \mu\, L}{A\, \Delta P}$$

where k is the permeability in millidarcies, Q is the average rate of fluid flow in cc's per second, μ is the viscosity of the fluid in centipoises at the temperature of measurement, L is the length of the core in cm., A is the cross-sectional area of the core in cm^2, and ΔP is the pressure difference across the specimen in atmospheres.

In order to assure that dissolution will occur it is important to know the degree of initial undersaturation of the pore fluid. It was necessary to adjust the testing environment to make up for the time factor and give tests of reasonable lengths. In view of the experimental difficulty in producing high flow rates in material with a low permeability, we have chosen to increase the degree of undersaturation above that usually found in nature by increasing the CO_2 partial pressure. The partial pressures used during testing were in excess of the usual natural values by about one to five orders of magnitude. Since the thermodynamic data on aqueous ions is not available for the testing conditions, the values at one atmosphere will be used to make an approximation of the $CaCO_3$ saturation concentration (C_{sat}) and thus the degree of undersaturation. First, the pCO_2 of the starting fluid will be calculated, which will be converted to CO_2 fugacity so that C_{sat} can be found. This will be done for the two initial CO_2 pressures used during testing (100 and 200 psi). The number of moles (M) of CO_2 placed in the circulator for each liter of volume can be calculated from the density of CO_2 using a molecular weight of 44. The densities (14 g/l and 26 g/l) are equivalent to 0.318 and 0.591 moles per liter. The density of water will be taken as a constant value of one g/cc, corresponding to 55.508 moles/liter. The mole fraction of the CO_2 is given by the relation:

$$X_{100} = \frac{M_{CO_2}}{M_{CO_2} + M_{H_2O}} = \frac{0.318}{0.318 + 55.508} = 0.00570$$

$$X_{200} = \frac{0.591}{0.591 + 55.508} = 0.01053\,.$$

X can be converted to partial pressure by use of Henry's law (ELLIS, 1959*a*) at 25°C:

$$pCO_{2\,100} = 1640\, X = 9.35 \text{ atm}$$

$$pCO_{2\,200} = 17.27 \text{ atm.}$$

At the pore pressure used during testing (5800 psi, 395 atm) CO_2 behaves non-ideally, and fugacity coefficient (α_{CO_2}) at this pressure is 0.18, so the fugacity at the start of the test ($f^\circ_{CO_2}$) was:

$$f^\circ_{CO_2\,100} = \alpha_{CO_2}\, pCO_2 = 0.18 \times 9.35 = 1.68 = 10^{0.225}$$

$$f^\circ_{CO_2\,200} = 0.18 \times 17.27 = 3.11 = 10^{0.493}.$$

Using the fugacity of CO_2, the solubility of calcite under experimental conditions can be calculated approximately by the method of GARRELS and CHRIST (1965, Chapter 3). If all of the solution in the circulator passes through the specimen, then the system can be considered closed (GARRELS and CHRIST, 1965, case 5). The calculation requires the use of the following chemical relationships:

$$CaCO_3 = Ca^{++} + CO_3^{=}$$

$$K_{11} = (Ca^{++})(CO_3^{=}) = 10^{-8.3}. \tag{1}$$

This equilibrium represents the solubility product for calcite (ELLIS, 1959*b*).

$$CO_{2(aq)} + H_2O = H_2CO_3$$

$$K_{15} = \frac{(H_2CO_3)}{pCO_{2(g)}} = 10^{-1.47} \tag{2}$$

In this case, the CO_2 concentration is expressed in partial pressure of the gas, and the equilibrium constant is so defined.

$$H_2CO_3 = H^+ + HCO_3^-$$

$$K_{16} = \frac{(H^+)(HCO_3^-)}{(H_2CO_3)} = 10^{-6.4} \tag{3}$$

This is the first acid dissociation of H_2CO_3.

$$HCO_3^- = H^+ + CO_3^{=}$$

$$K_{17} = \frac{(H^+)(CO_3^{=})}{(HCO_3^-)} = 10^{-10.3} \tag{4}$$

This is the second acid dissociation of H_2CO_3.

$$H_2O = H^+ + OH^-$$

$$K_{58} = (H^+)(OH^-) = 10^{-14.} \tag{5}$$

This is the dissociation reaction for water.

The carbonic acid concentration of the initial fluid can be obtained from equation 2, using fugacity instead of partial pressure:

$$(H_2CO_3)^\circ_{100} = 10^{-1.47} \times f^\circ_{CO_2} = 10^{-1.245}$$
$$(H_2CO_3)^\circ_{200} = 10^{-0.977}.$$

The charge balance is:

$$(H^+) = (HCO_3^-) + 2\,(CO_3^=). \tag{6}$$

At moderate values of pH, $(CO_3^=)$ is much less than (HCO_3^-), so equation 6 becomes:

$$(H^+) = (HCO_3^-). \tag{7}$$

Combining equations 3 and 7 gives the result:

$$\frac{(H^+)^2}{(H_2CO_3)} = 10^{-6.4}. \tag{8}$$

The values of (H^+) calculated from equation 8 are $10^{-3.82}$ (100 psi) and $10^{-3.69}$ (200 psi). The total dissolved carbonate (ΣCO_3) at the start of the test is:

$$\Sigma CO_3^\circ{}_{100} = (H_2CO_3) + (HCO_3^-) = 10^{-1.245}$$
$$\Sigma CO_3^\circ{}_{200} = 10^{-0.987}.$$

As calcite dissolves, each Ca^{++} ion released to the solution is accompanied by a $CO_3^=$ ion, which may be converted to HCO_3^- or H_2CO_3, so the total carbonate after dissolution will equal the total carbonate before dissolution plus the Ca^{++} concentration:

$$(Ca^{++}) + \Sigma^\circ_{CO_3} = (H_2CO_3) + (HCO_3^-) + (CO_3^=). \tag{9}$$

The solution must be electrically neutral, so:

$$2\,(Ca^{++}) + (H^+) = (HCO_3^-) + (OH^-) + 2\,(CO_3^=). \tag{10}$$

This gives six variables ((Ca^{++}), (H^+), (H_2CO_3), (HCO_3^-), $(CO_3^=)$ and (OH^-)) and six equations (1, 3, 4, 5, 9, and 10). As a first approximation, the values of $(CO_3^=)$, (H^+) and (OH^-) in equations 9 and 10 can be considered negligible compared to the others. The set of equations can then be solved by converting all values to

(H^+), giving a fourth power polynomial in (H^+) which is solved by trial and error. Back substitution gives the values for all of the variables:

		100 psi	200 psi
(H^+)	=	$10^{-5.86}$	$10^{-5.68}$
(HCO_3^-)	=	$10^{-1.78}$	$10^{-1.70}$
(H_2CO_3)	=	$10^{-1.24}$	$10^{-0.98}$
(OH^-)	=	$10^{-8.1}$	$10^{-8.3}$
$(CO_3^=)$	=	$10^{-6.22}$	$10^{-6.32}$
(Ca^{++})	=	$10^{-2.075}$	$10^{-1.98}$

This indicates equilibrium pH values of 5.86 and 5.68, C_{sat} of 0.84 and 1.04 g/l, and ionic strengths of 0.025 and 0.031, and shows that the assumption of low values for $(CO_3^=)$, (H^+) and (OH^-) was justified.

The ionic strengths above are sufficiently great that the activity coefficients are not unity, and must be considered in the calculations. Equations 1, 3, 4, and 5 remain valid, but equations 9 and 10 must be replaced by:

$$\frac{(Ca^{++})}{\gamma Ca^{++}} + \Sigma^{\circ}_{CO_3} = (H_2CO_3) + \frac{(HCO_3^-)}{\gamma HCO_3^-} + \frac{(CO_3^=)}{\gamma CO_3^=} \tag{11}$$

and:

$$\frac{2\,(Ca^{++})}{\gamma Ca^{++}} + (H^+) = \frac{(HCO_3^-)}{\gamma HCO_3^-} + (OH^-) + \frac{2\,(CO_3^=)}{\gamma CO_3^=}. \tag{12}$$

With the approximation that γ_{H^+}, γ_{OH^-}, and $\gamma_{H_2CO_3}$ are unity, the equations are solved in the same way as above. The activity coefficients are determined by estimating the final ionic strength and γ values (GARRELS and CHRIST, 1965, p. 63 and 104), solving for more accurate values of I and γ_i, and repeating until the calculated I and the estimated I are the same. This gives the result:

		100 psi	200 psi
(H^+)	=	$10^{-5.95}$	$10^{-5.78}$
(HCO_3^-)	=	$10^{-1.69}$	$10^{-1.60}$
(H_2CO_3)	=	$10^{-1.24}$	$10^{-0.98}$
(OH^-)	=	$10^{-8.05}$	$10^{-8.22}$
$(CO_3^=)$	=	$10^{-6.04}$	$10^{-6.12}$
(Ca^{++})	=	$10^{-2.25}$	$10^{-2.18}$

where all values are in activities. This indicates final pH values of 5.95 and 5.78, ionic strengths of 0.030 and 0.040, and $CaCO_3$ saturation concentrations of 1.03 and 1.31 g/l for the two cases. Consideration of the activity coefficients in this situation has led to a slight increase in C_{sat} over the results obtained without activity coefficients.

Another possibility is that the first small amount of fluid passing through the specimen may be supplied with additional H_2CO_3 from the fluid still in the circulator. This would occur if the rate of diffusion of H_2CO_3 was large relative to the flow rate. However, since the values of (H_2CO_3) before and after dissolution are about the same, then the concentration variation between the sample and the circulator would be small, and the amount of diffusion would be negligible. Likewise, Ca^{++} ions may migrate from the sample chamber to the circulator. This would increase the amount of carbonate which could be dissolved by the first increment of fluid circulated.

In summary, if all of the solution in the circulator (1080 cc) passes through the specimen, it would have the potential to dissolve about 1.1 or 1.4 grams of $CaCO_3$, depending on the initial CO_2 pressure. If this much carbonate were actually dissolved, then a specimen ½ inch in diameter and length would have a porosity increase of 25% and 32%.

Results of Experimentation

The results of the eleven tests run are presented in two ways. A description of each test gives the length of the test, the amount of fluid circulated, the specimen porosity increase by weight loss, and a description of the results of testing. Also, a graph of each test shows the amount of fluid flowed, the pore pressure differential, and the specimen permeability, all plotted against time. Note that the scale changes between different plots.

Test DR-1

This test was the first of a series to evaluate the effect of specimen orientation on the test results. The progress of the test is illustrated in Figure 4. The specimen was oriented so that the flow direction was horizontal through the rock. The pore pressure differential was allowed to increase by running the gear pump in fifth gear with the intensifier, reaching a maximum of 300 psi after 39.75 hours before dropping off sharply. Circulation was then continued for 54.5 more hours. A total of 70.9 cc of fluid was circulated and the specimen lost 0.095 g in weight, equivalent to an average concentration in the effluent of 1.34 g/l. The specimen gained 2.2% in porosity, from 12.1 to 14.3% (calculated from densities). The permeability of the specimen increased slowly for the first 30 hours of the test, then increased drastically at the point where the pore pressure dropped to zero.

After testing the core showed four types of porosity, three of which were present prior to testing and one which resulted from the testing. All of the ooids showed a uniform light blue color in reflected light resulting from microporosity in the cortical layers which was present before testing. All other tested specimens also showed this feature. This blue tint is absent from the sparry calcite cement and from some bioclasts, especially echinoderms, indicating the lack of microporosity in those

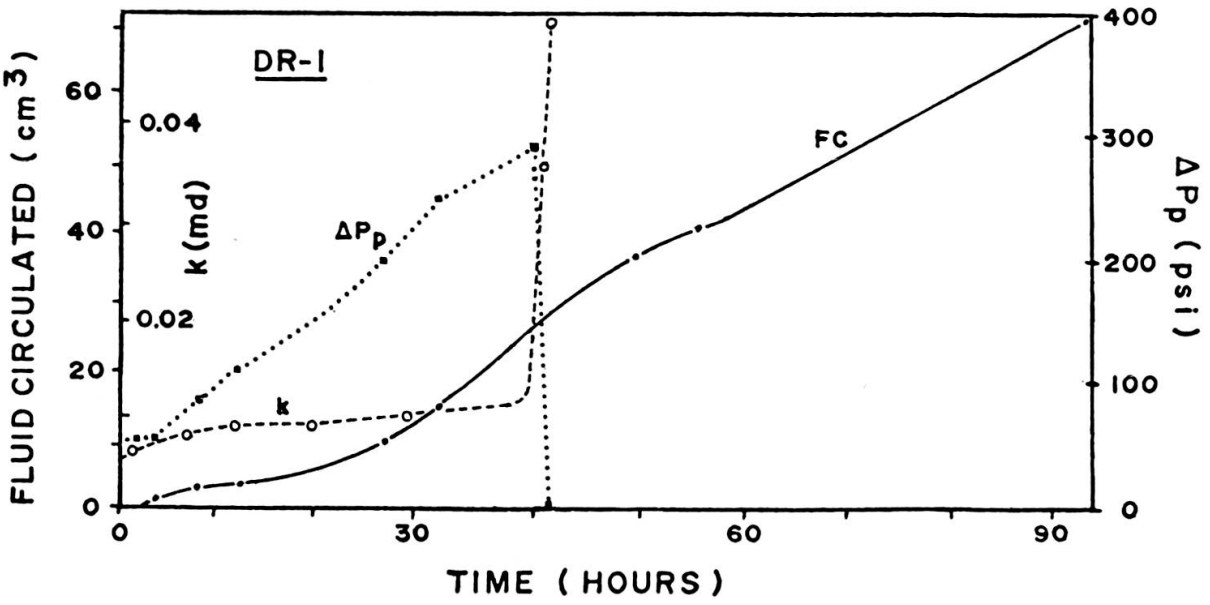

FIG. 4. — Experimental results, test DR-1.

components. Scattered throughout the sparite cement are pores ranging in size from 20 to 125 μm which are due to incomplete cementation and which were also present prior to testing. These pores are probably non-interconnected on this scale and communicate only through the ooid microporosity. The third type of pore common to all specimens before and after testing is located preferentially near the outer cortical layers of the ooids. This pore type ranges in size from 20 × 125 μm to 50 × 250 μm. This pore type is usually located within an area interior to a spalled cortical layer. Less commonly this type of pore is located irregularly within the ooid cortex, and in this case, may be partly due to testing.

The most prominent pore type present after testing is a single large channel 1-2 mm wide extending the entire length of the specimen from top to bottom (Plate 2, Fig. 5). The channel shows some fabric selectivity along the margins favoring dissolution of ooids over cement, with several triangular protrusions of cement into the channel. One partial ooid toward the bottom (outflow) side of the specimen shows evidence of having moved after dissolution (Plate 2, Fig. 6) suggesting some mechanical contribution to channel formation.

Test DR-2

This was also a horizontal specimen and the ΔP_p was controlled in the same manner as for Test DR-1. The progress of the test is illustrated in Figure 5. The ΔP_p increased to a maximum of 280 psi after 30 hours, then decreased to about 240 psi before dropping off sharply after a total of 49.5 hours, and the test was ended within one hour. 41.1 cc of fluid was circulated and the specimen lost 0.081 g for an average of 1.97 g/l. The porosity increased 2% from 11.7 to 13.7%. The permeability

maintained a constant value for most of the test, then after 33 hours began to increase, slowly at first and then more rapidly, at the same time that the ΔP_p was dropping off.

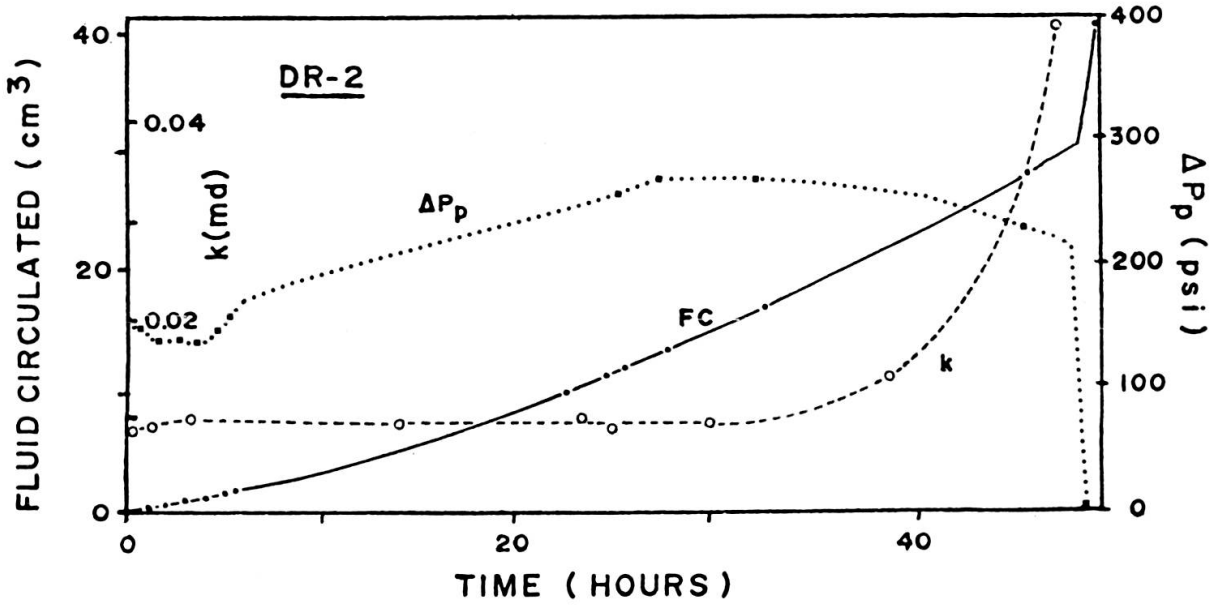

FIG. 5. — Experimental results, test DR-2.

The tested core shows an irregular channel less than 1 mm across, located almost entirely within the original boundaries of ooids, with several triangular remnants of sparite protruding into the channel.

Test DR-3

This test was on a vertically oriented specimen, run for comparison with the two previous tests. The gear pump and intensifier were used as before, and after some initial variation the ΔP_p leveled off at a constant value for most of the test, then dropped drastically near the end (Fig. 6). The test was run for 26.25 hours, 27.51 cc of fluid was circulated, and the specimen lost 0.011 g for an average of 0.4 g/l. The porosity increased 0.26% from 11.74 to 12.00%, and the permeability increased slowly for most of the test, then rapidly at the end.

The core after testing showed one or possibly two irregular small channels about 100 μm in width, mostly located within former ooids but with some sparite removed between grains (Plate 2, Fig. 4). The channeling meanders into and out of the plane of the thin section but probably extends the whole length of the specimen.

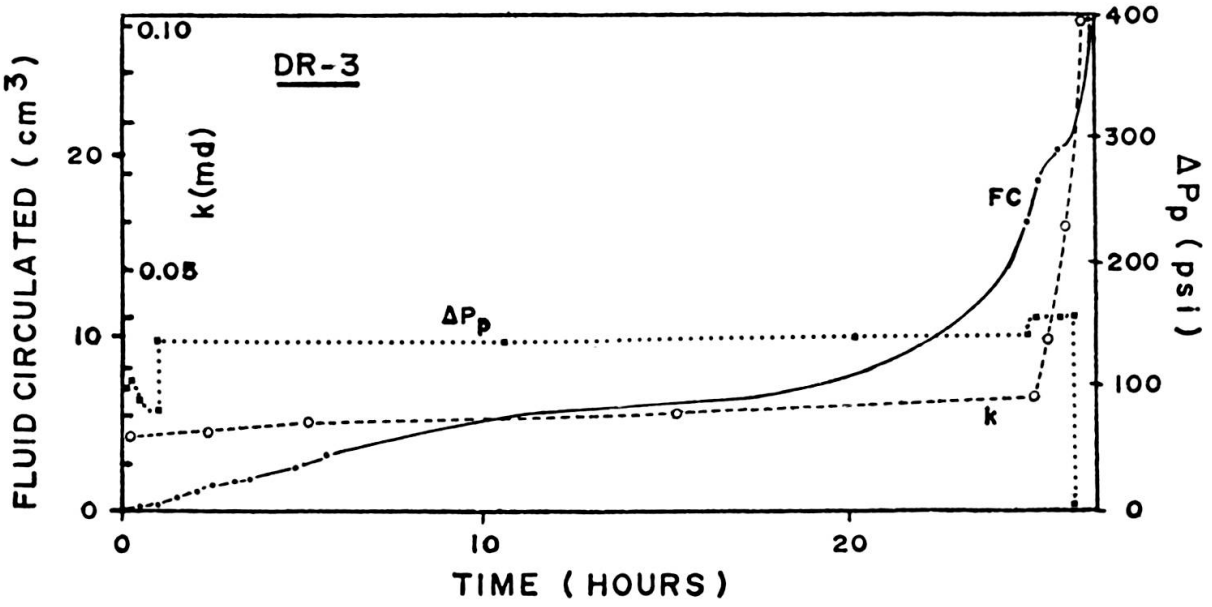

FIG. 6. — Experimental results, test DR-3.

Test DR-4

This test was also performed with a vertically oriented specimen, run in the same way as the previous three (Fig. 7). It lasted 104.5 hours, 76.38 cc of fluid were circulated, and the specimen lost 0.069 g in weight for an average of 0.9 g/l. The porosity increased 1.65% from 11.50 to 13.15%. The permeability showed an initial small decrease, possibly due to compaction of the filter paper discs in the specimen

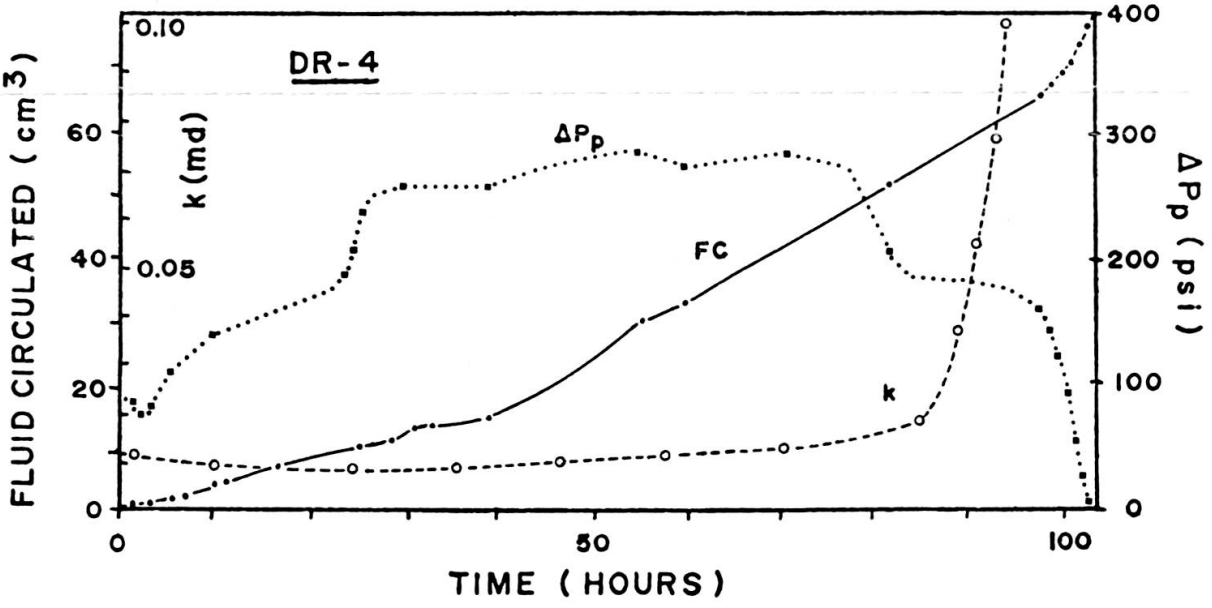

FIG. 7. — Experimental results, test DR-4.

assembly. This decrease was followed by a gradual increase, then a sudden increase as the ΔP_p dropped off.

The tested specimen shows a single channel which is discontinuous in the plane of the thin section, with bridges remaining between the pores. These bridges are composed of the less porous outer cortical layers and the interparticle cement (Plate 2, Fig. 3). This gives a crude version of oomoldic porosity.

Test DR-5

This test and each of the remaining ones was run on a horizontally oriented core. The initial CO_2 pressure in the circulator was decreased from 200 psi to 100 psi to bring the test conditions closer to natural ones and to see if variations in the pCO_2 changed the results. The pump was run continuously as in the previous tests, and the ΔP_p increased gradually then decreased, gradually at first, then drastically (see Fig. 8). The permeability showed an initial increase, a decrease, a gradual increase, then a sharp increase when the pore pressure dropped suddenly. The test lasted 66.9 hours, 48.88 cc of fluid was circulated, and the specimen weight loss was 0.080 g, for an average of 1.6 g/l. The porosity increased 1.9% from 10.5 to 12.4%.

After testing, the specimen showed a more even distribution of porosity enhancement than in previous tests, with numerous small channels visible on the top of the core and none on the bottom. In thin section one of the channels is bordered in one area by cleavages of the calcite spar, suggesting that mechanical failure contributed to channel formation.

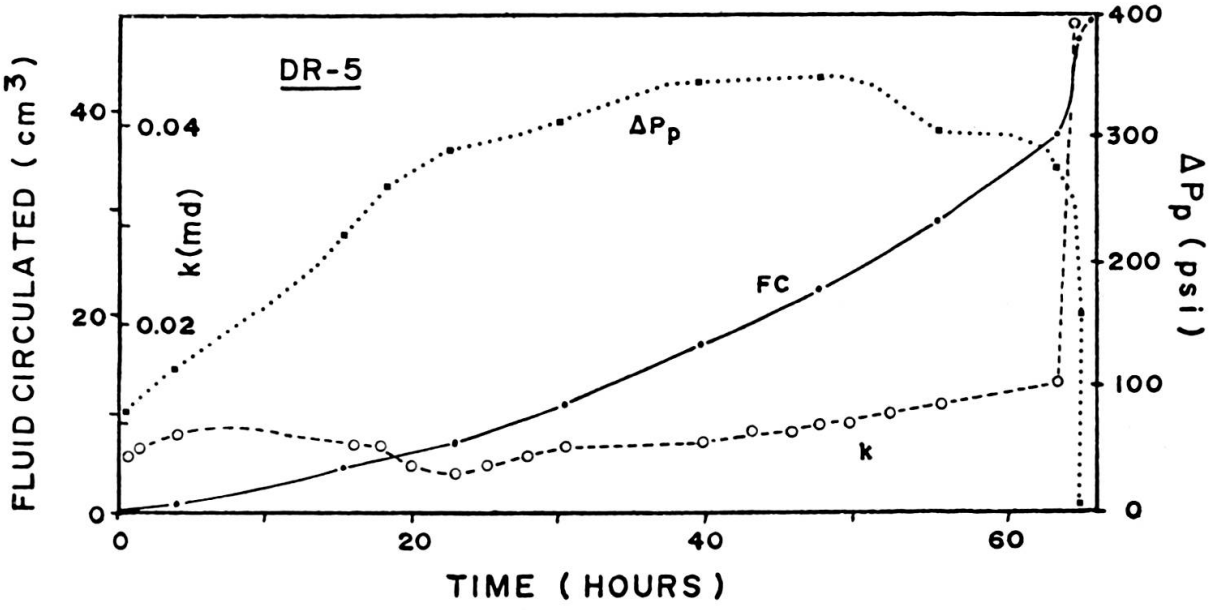

FIG. 8. — Experimental results, test DR-5.

Test DR-6

This test (Fig. 9), with an initial CO_2 pressure of 200 psi, was run for 45.17 hours, with 40.09 cc of fluid circulated and a specimen weight loss of 0.052 g or 1.3 g/l. The porosity increased 1.4% from 10.7 to 12.1%. The pore pressure differential

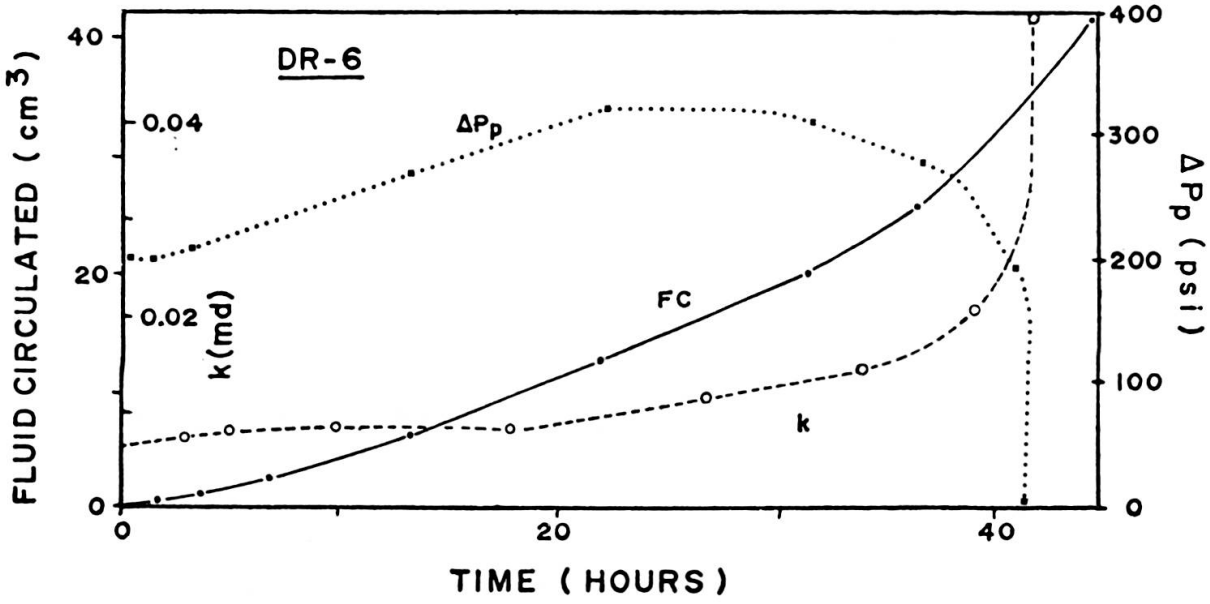

FIG. 9. — Experimental results, test DR-6.

increased during the first part of the test, then decreased, slowly at first then gradually faster until reaching zero. The permeability increased throughout the test, slowly at first, then at a gradually increasing rate as the ΔP_p dropped off.

The tested specimen showed several small channels, mostly within ooid cortex material. No evidence of mechanical breakage was noted.

Test DR-7

This test was run for a short time (27.7 hours) and with the lower initial CO_2 pressure (100 psi) in an attempt to avoid channeling. The test was ended after the first indication of a permeability increase (Fig. 10); 9.81 cc of fluid was circulated and the specimen lost 0.020 g in weight for an average of 2.0 g/l, more than two times the value that C_{sat} for this CO_2 pressure would have been if all of the solution had been circulated. The specimen had a porosity increase of 0.4% from 10.5 to 10.9%.

The core after testing showed no channels, and dissolution appears to have been limited to some areas interior to spalled cortical layers.

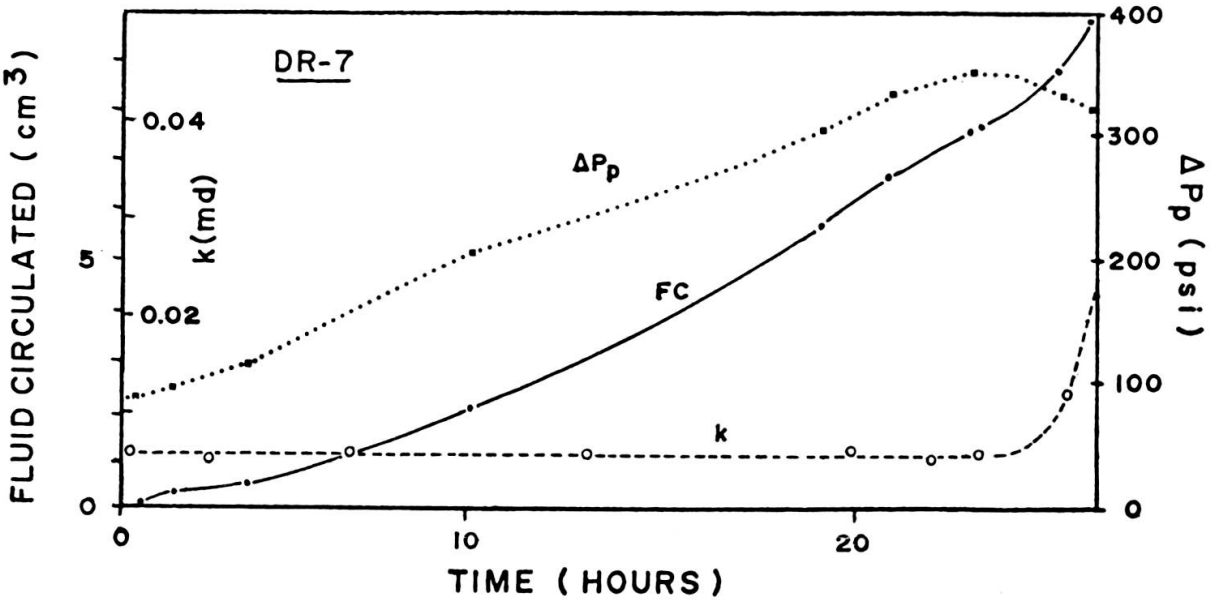

FIG. 10. — Experimental results, test DR-7.

Test DR-8

The purpose of this test (Fig. 11) was to see if prolonged testing would produce more pronounced results. It was run for 1111.7 hours and 834.4 cc of fluid was circulated producing a weight loss of 0.108 g or 0.13 g/l, and a porosity increase of 2.7%, from 10.4 to 13.1%. The gear pump was run at a constant rate and ΔP_p increased at first then dropped off gradually. The permeability increased irregularly throughout the test.

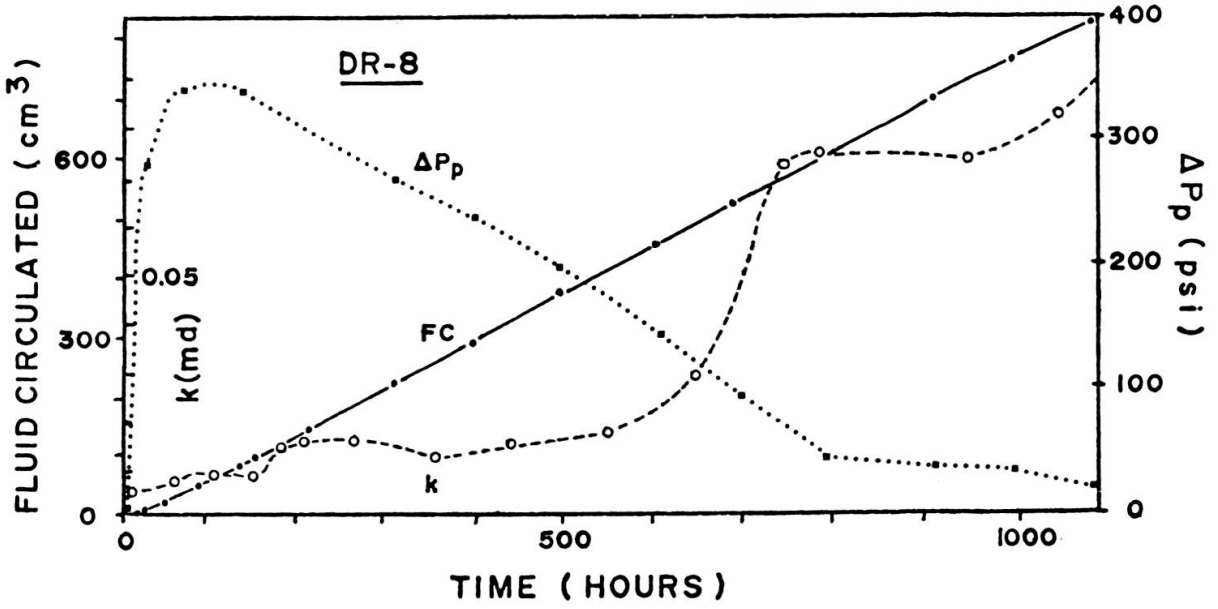

FIG. 11. — Experimental results, test DR-8.

The tested core showed one channel with oomoldic to vuggy margins. Apparently whatever dissolution features may have formed were mostly destroyed by enlargement of the channel.

Test DR-9

In this test the gear pump was controlled automatically to maintain the ΔP_p at a constant value of 50 psi (Fig. 12). After about 50 hours of testing the flow rate decreased drastically and the permeability also dropped, from the starting value of 0.002 millidarcies to an extremely low value of 0.00005 millidarcies. After 3902.5 hours

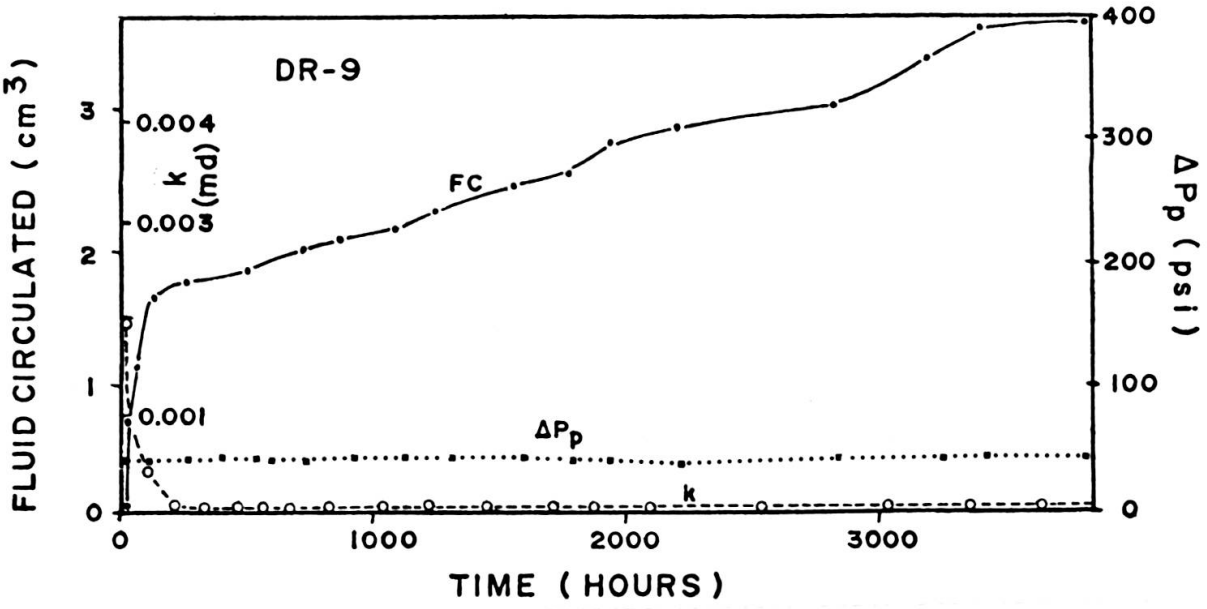

FIG. 12. — Experimental results, test DR-9.

(about 162 days) only 3.626 cc of fluid had been circulated, and the test was terminated. After testing the sample weighed 0.066 g more than prior to testing. No explanation for this unusual behavior has been found. No foreign material could have passed from the circulator system through the filter paper and into the specimen, and the weight gain has been corrected for jacket weight loss. Petrographically, the specimen showed no porosity resulting from testing.

Test DR-10

This test was run to see if variations in the ΔP_p would lead to different results. To do this, the gear pump was turned on and off once daily, causing the ΔP_p to vary between 50 and 150 psi (Fig. 13). The test was run for 189 hours, and 56.7 cc were circulated. The specimen lost 0.069 g in weight for an average of 1.2 g/l, and had a

PLATE I

FIG. 1. — Thin section of typical oolitic calcarenite with scattered mesoporosity (in black).

FIG. 2. — Pore cast of the same specimen showing fine microporosity of ooid cortex and coarser microporosity of micrite lithic cores.

FIG. 3. — Detail of pore cast of ooid microporosity with irregular pore shape resulting from imprint of small calcite rhombohedra which make up the cortical layers.

FIG. 4. — Pore cast revealing connection between intercrystalline pores and ooid microporosity.

FIG. 5. — Thin section of foraminifer *Endothyra* sp. with characteristic dark micritic wall.

FIG. 6. — Pore cast of a similar foraminifer showing microporosity located in the wall which is similar in appearance to ooid cortex microporosity.

PLATE 2

FIG. 1. — Early stage of dissolution showing irregular preferential dissolution of cortical layers near but not at grain surfaces.

FIG. 2. — Contact between two intraparticle pores at a grain contact.

FIG 3. — Series of several intraparticle pores separated by thin partitions, indicating that at this stage mechanical bursting has not occurred.

FIG. 4. — A string of intraparticle pores connected at grain contacts and avoiding the cement.

FIG. 5. — Final stage of dissolution/breaking, where both grains and cement have been removed in a channel.

FIG. 6. — Close-up of a channel margin showing a dislocated fragment (center) which has moved towards the lower right and rotated slightly. This movement demonstrates a mechanical contribution to carbonate removal in this case.

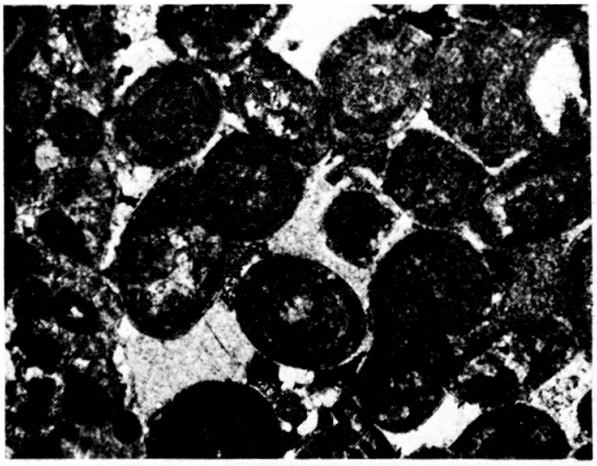

Fig. 1 OR4A 1mm XN

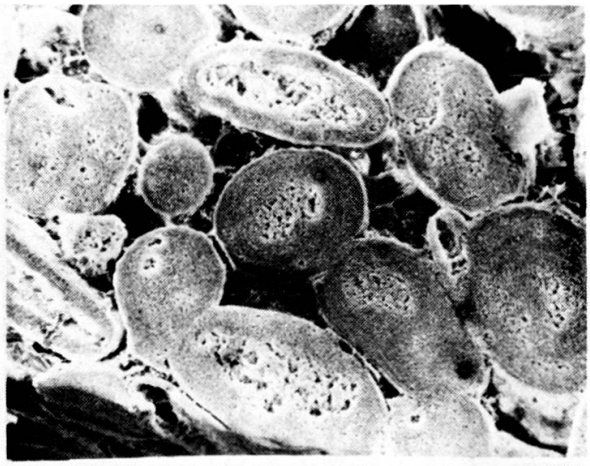

Fig. 2 OR4A 100 µm SEM

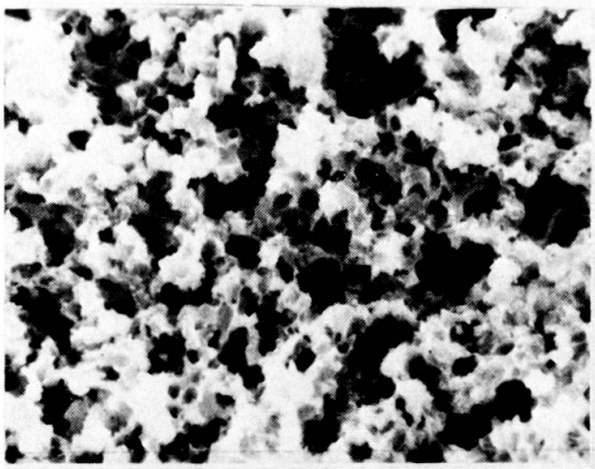

Fig. 3 OR4A 10 µm SEM

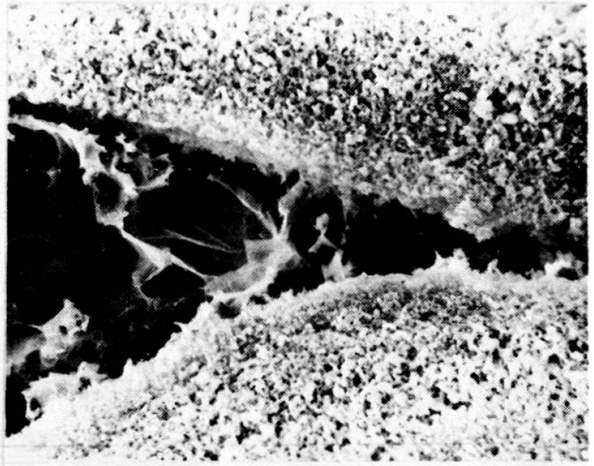

Fig. 4 OR4A 10 µm SEM

Fig. 5 OR4A 100 µm PL

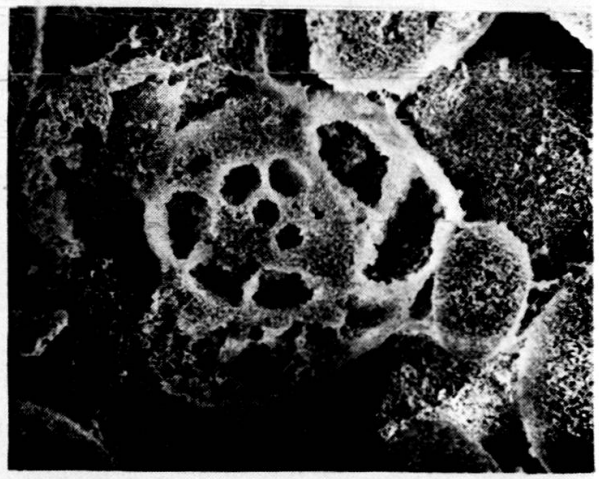

Fig. 6 OR4A 100 µm SEM

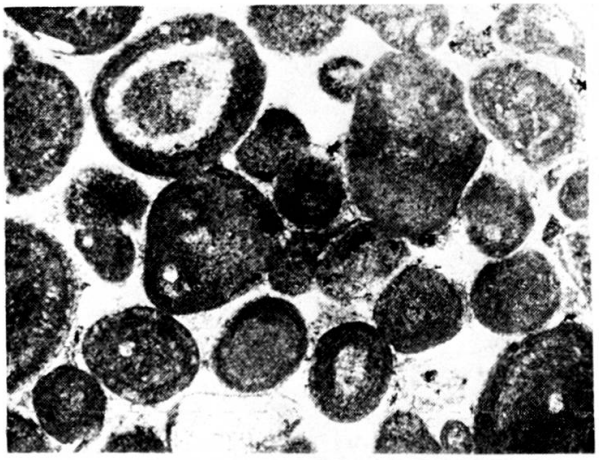

Fig. 1 DR10 1mm XN

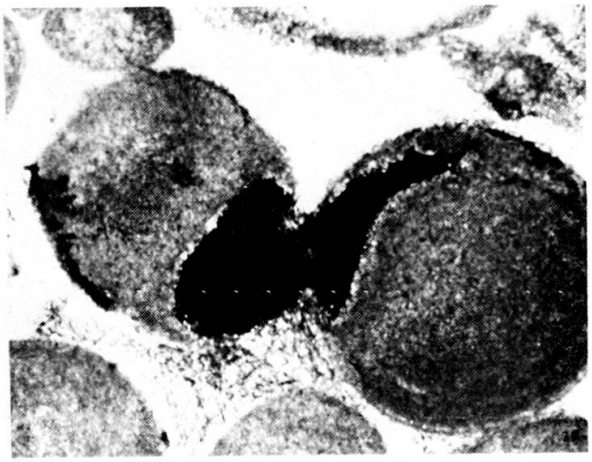

Fig. 2 DR11 100μm XN

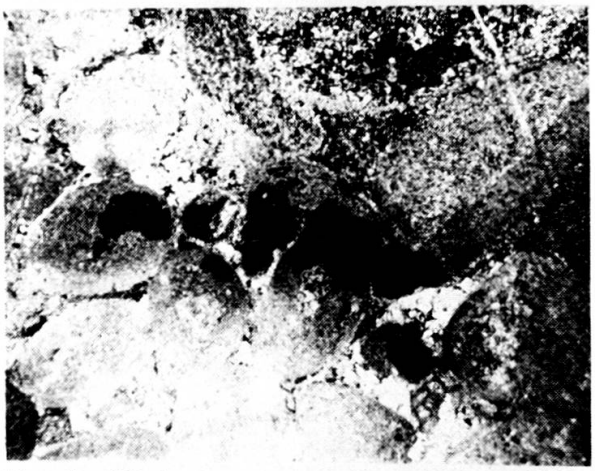

Fig. 3 DR4 1mm XN

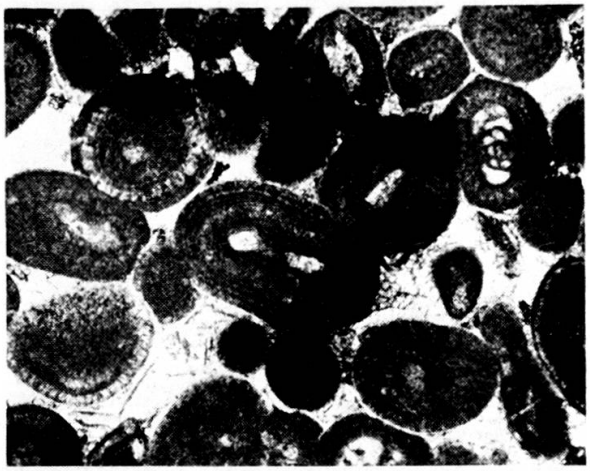

Fig. 4 DR3 1mm XN

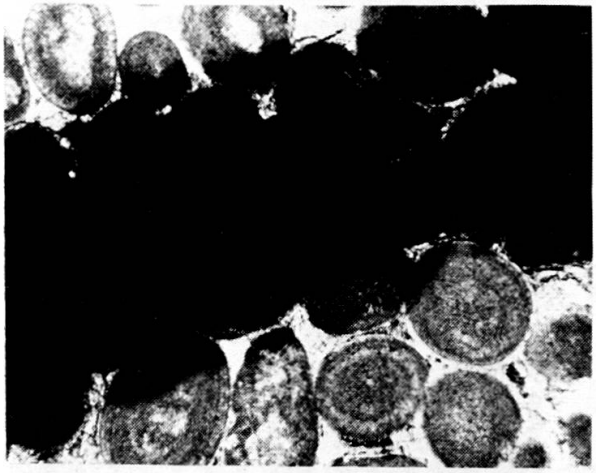

Fig. 5 DR1 1mm XN

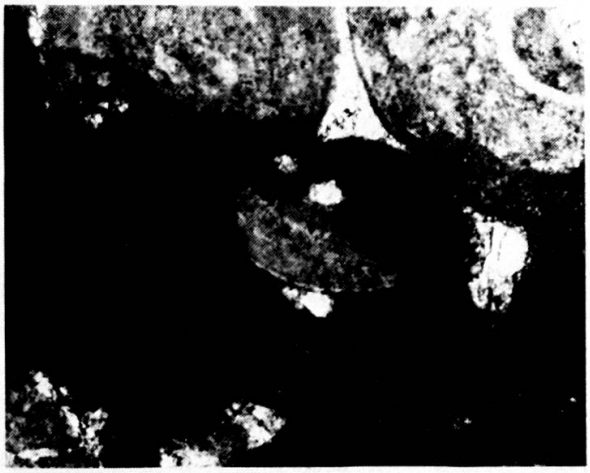

Fig. 6 DR1 100μm XN

porosity increase of 1.6% from 10.5 to 12.1%. The permeability showed an initial slight decrease, then a moderate and then rapid increase, then another decrease followed by a moderate and then a drastic increase as the ΔP_p dropped to zero. The reason for the hump in the permeability curve after 110 hours of testing is not known, but it is related to an increase in the flow rate and a decrease in the ΔP_p which occurred at about the same time.

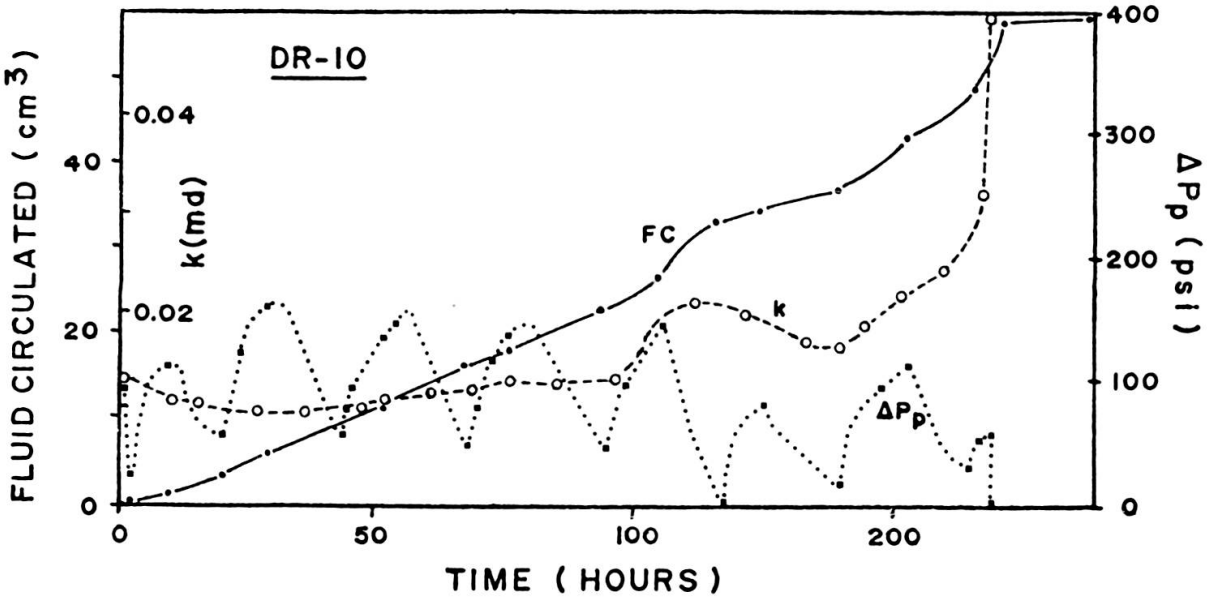

FIG. 13. — Experimental results, test DR-10.

After testing the specimen showed several localized areas of porosity enhancement, with dissolution confined to the inner cortical layers of some of the ooids, leaving the outermost layers and the interparticle sparite (Plate 2, Fig. 1).

Test DR-11

This test was run with automatic controls on the ΔP_p keeping it at a constant value of 150 psi for 400 hours, then decreasing it to 100 psi for the remainder of the test (Fig. 14). The test lasted 698.5 hours, 82.23 cc of fluid was circulated, and the specimen lost 0.016 g in weight, or 0.19 g/l. The porosity increased 0.4% from 13.0 to 13.4%, and the permeability increased gradually throughout the test.

The tested core shows a single channel 1 mm wide which is not-fabric-selective, and which extends about one half the length of the specimen. It then becomes an irregular fabric-selective channel passing from ooid to ooid at grain contacts and passing into and out of the plane of the thin section (Plate 2, Fig. 2).

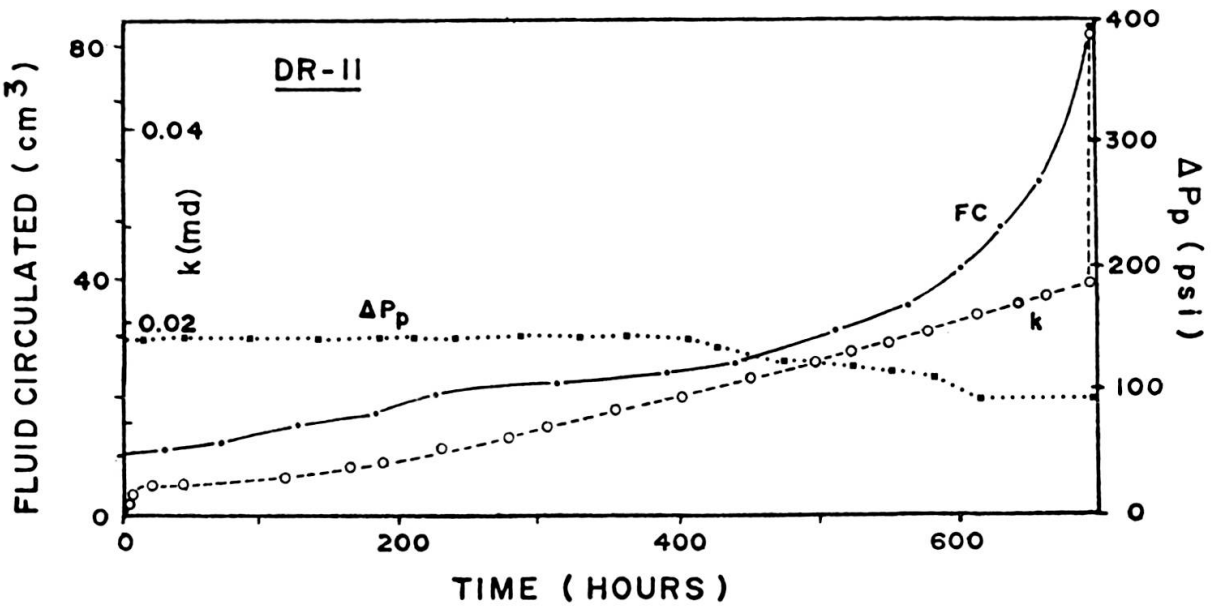

FIG. 14. — Experimental results, test DR-11.

Accuracy

The following are the accuracies of the various measurements and derived values. The accuracies are theoretical maximum errors based on the accuracy of the measuring instruments, and are presented as percent of the measured (or derived) value. The accuracy of derived values was obtained by adding the percent errors of all of the values used in the calculation. The pore pressure difference was measured to $\pm 3\%$; the volume of fluid circulated, $\pm 1\%$; the time, $\pm 0.4\%$; and the specimen weight loss $\pm 10\%$. The porosity had a combined error of $\pm 0.34\%$ and the porosity increase, $\pm 10.3\%$. The accuracy of the permeability measured during testing cannot be stated since the value of the viscosity is not known and an arbitrary value of one centipoise was used. However, the combined error of the other terms used in the calculation was $\pm 4.7\%$.

CONCLUSIONS

The conclusions reached from the series of systematic tests have modified some of the preliminary results with respect to the effects of variations of pore pressure differential. They are as follows:

1) Variation of the specimen orientation, using horizontally and vertically oriented cores from the original outcrop specimen, caused no change in the experimental results. This is not surprising, since the oolitic limestone used was massive and showed no bedding or other feature which could have made it anisotropic.

2) Variation of the pCO_2 caused little or no change in the experimental results for the two values used (9.35 and 17.27 atm). As long as the solution is undersaturated it will dissolve any carbonate it contacts. The degree of undersaturation will control the rate and amount of dissolution, but the location of the dissolution is controlled by fluid access.

3) Variations in the ΔP_p did change the outcome of the tests. Tests with low values of ΔP_p showed less tendency for channeling and more even distribution of porosity enhancement. The test in which the ΔP_p was varied between 0 and 150 psi (DR-10) had the same outcome as the one where the ΔP_p was maintained at 150 psi for the entire test (DR-3). Apparently, whether or not a channel forms depends on the maximum value of the ΔP_p near the end of the test, when the specimen has been weakened by dissolution.

4) It was found that tests in which the ΔP_p showed a sudden drop and the permeability a sudden increase also showed channeling. Two of the channels exhibited features indicating a mechanical origin for the channel. Tests which had no sudden ΔP_p drop showed no channels or evidence of breakage. It is therefore concluded that the channel involves a mechanical bursting of an area of the specimen which has been weakened by dissolution, and that the channeling destroys most of the dissolution texture.

5) Several of the tests showed specimen weight losses greater than would be expected given the amount of fluid circulated and the degree of undersaturation. All but one of these tests showed evidence of mechanical breakage, and material removed in this way could explain the discrepancy for those cases. Test DR-7 showed a specimen weight loss for the fluid circulated of 2.0 g/l, while the initial degree of undersaturation was only 1.03 g/l. This suggests that there was some replenishment of undersaturation by diffusion of Ca^{++} ions upstream to the circulator. This diffusion cannot be evaluated quantitatively since the diffusion coefficient under test conditions, especially through the porous discs and filter paper, is not known. The results of Test DR-7 indicate that diffusion is important in increasing the apparent degree of undersaturation when only part of the fluid in the circulator is used.

6) The generation of oomoldic secondary porosity is confirmed and takes place by differential dissolution of the microporous ooids, leaving the sparite cement unaffected. It is possible to combine the results of all the tests into an ideal sequence of specimen reaction to circulation of an undersaturated solution. At the start of the test the pore fluid flows through the microporosity of the ooids, from grain to grain, avoiding the sparite cement. Dissolution begins with some of the inner, porous cortical layers (Plate 2, Fig. 1). The dissolution continues and the newly formed mesopores begin to link up at grain contacts (Plate 2, Fig. 2), eventually

forming chains of pores with some partitions remaining in between (Plate 2, Fig. 3). As dissolution continues, the partitions are removed and the pores link up into a continuous fluid path (Plate 2, Fig. 4). What happens next depends on the ΔP_p across the specimen. If the pressure is sufficiently high, the specimen will burst and a channel will form which is not-fabric-selective (Plate 2, Figs. 5 and 6). This channel destroys any texture which may have formed previously. Continued circulation may further dissolve the margins of the channel. If a channel does not form, dissolution proceeds inside the ooids until their complete removal and oomoldic porosity is generated with the sparite cement untouched.

LIST OF REFERENCES

CARR, D. D. (1973). Geometry and origin of oolite bodies in the Ste. Genevieve Limestone (Mississippian) of the Illinois Basin: *Indiana Geological Survey Bulletin 48*, 81 p.

DONATH, F. A., A. V. CAROZZI, L. S. FRUTH, Jr. and D. W. RICH (1976). Experimental development of permoporosity in carbonate rocks (Abstract): *Bull. Am. Assoc. Petroleum Geologists*, v. 60, 4, pp. 665-666.

—— (1977). Fabric-selective permoporosity experimentally developed in carbonate rocks (Abstract): *Bull. Am. Assoc. Petroleum Geologists*, v. 61, 5, p. 781.

—— (1980). Oomoldic porosity experimentally developed in Mississippian oolitic limestone: *Jour. Sed. Petrology*, v. 50, 4, 1249-1259.

ELLIS, A. J. (1959*a*). The solubility of carbon dioxide in water at high temperatures: *Am. Jour. Science*, v. 257, pp. 217-234.

—— (1959*b*). The solubility of calcite in carbon dioxide solutions: *Am. Jour. Science*, v. 257, pp. 354-365.

GARRELS, R. M. and C. L. CHRIST (1965). *Solutions, minerals and equilibria:* Freeman, Cooper and Co., San Francisco, 450 p.

HISELER, R. B. and A. V. CAROZZI (1978). A testing of permeability estimation techniques in oolitic calcarenites, Ste. Genevieve Limestone (Mississippian), Southern Illinois: *Archives des Sciences*, v. 31, 2, pp. 87-128.

RICH, D. W. (1980). Porosity in oolitic limestones: *Unpublished Ph.D. dissertation University of Illinois at Urbana-Champaign*, 185 p.

SCHMIDT, V. and D. A. MCDONALD (1979). The role of secondary porosity in the course of sandstone diagenesis: *in* P. A. Scholle and P. R. Schluger (eds.), *Aspects of diagenesis:* S.E.P.M. Special Publ. No. 26, pp. 175-207.

WARDLAW, N. C. (1976). Pore geometry of carbonate rocks as revealed by pore casts and capillary pressure: *Bull. Am. Assoc. Petroleum Geologists*, v. 60, 2, pp. 245-257.